PAPERS

Low-temperature facile synthesis of graphene and graphene-carbon nanotubes hybrid on dielectric surfaces

Materials Research
Express

Low-temperature facile synthesis of graphene and graphene-carbon nanotubes hybrid on dielectric surfaces

Cheng Yang[1], Chao Zhang[1], Gang Zhang[2], Hua-Min Li[2], Ru-Jun Ma[2], Shi-Cai Xu[1], Shou-Zheng Jiang[1], Mei Liu[1] and Bao-Yuan Man[1]

[1] College of Physics and Electronics, Shandong Normal University, Jinan 250014, People's Republic of China
[2] Sungkyunkwan University Advanced Institute of Nano-Technology (SAINT), Sungkyunkwan University, Suwon 440-746, Korea
E-mail: chengyang@sdnu.edu.cn and byman@sdnu.edu.cn

Received 18 December 2013, revised 27 January 2014
Accepted for publication 29 January 2014
Published 7 March 2014

Materials Research Express **1** (2014) 015607

doi:10.1088/2053-1591/1/1/015607

Abstract

Various carbon based nanostructures (graphene, graphene-CNTs hybrid and three-dimensional (3D) carbon network) have been grown separately on low-temperature (600 °C) substrates by using a chemical vapor deposition system with a two-heating reactor. The two-heating reactor is utilized to offer sufficient, well-proportioned floating C atoms and provide a simple method for low-temperature deposition. Morphology and electrical properties of the carbon based nanostructures can be controlled by the substrate surfaces. A relatively flat surface is beneficial for the synthesis of graphene and surfaces with nanodots are required to directly grow graphene-carbon nanotube hybrids. A chemical vapor deposition mechanism dependent on the temperature gradient is proposed, suggesting that the transfer-free carbon nanostructures can be deposited on different substrates. These results open an easy way for direct and high-efficiency deposition of various carbon nanostructures on the low-temperature dielectric substrates.

Keywords: graphene, graphene-CNTs hybrid, mechanism, active catalytic site

1. Introduction

Carbon nanostructures, including carbon nanotubes (CNTs) and graphene are envisaged as key materials in postsilicon electronics. CNTs have been reported by numerous papers on the growth [1–6], properties [7–9], and applications [10–12]. Graphene has also been paid special

attention owing to its unique properties and potential applications in the areas of transparent electrodes [13], ultrasensitive sensors [14], field-effect transistors [15] as well as energy storage [16] and conversion [17]. In order to combine the advantages of graphene and CNTs, many attempts have recently been made to prepare graphene-CNT hybrid materials or other-types of 3D nanomaterials. Using a solid-phase layer-stacking approach, Li and co-workers assembled freestanding composite thin films of CNTs and graphene, which were used in highly transparent/conductive thin film applications [18]. Das *et al* reported controlled growth of a self-organized graphene-CNTs hybrid structure and a single-step transfer process on to a flexible substrate [19]. By the electrochemical exfoliation method, Seo *et al* fabricated CNTs/graphene nanosheet composites [20]. A graphene-CNT hybrid has also been obtained using one-step CVD growth on Si nanoparticle coated copper foil [21]. Recently, structures consisting of micro- and nanofabricated carbon based graphene or graphene-CNT hybrid networks have been introduced as effective structures for the applications of supercapacitor [22, 23], microfluidic [24], dielectrophoresis [25], and batteries [26, 27]. These systems allow for considerable increases in the contact area, thus enhancing the electrical properties or the filtration and capture efficiency of nanoparticles and chemical materials. Here, we offer a novel chemical vapor deposition (CVD) method for the low-temperature growth of graphene and graphene-CNT hybrids using a two-heating reactor and provide a broader and deeper insight, discussing in detail the substrate surface effects for the growth of carbon based nanostructures in this case.

2. Experimental method

The experiment was carried out in the quartz tube horizontally located in the furnace with a two-heating reactor. As depicted in figure 1, one $8 \times 20\,cm^2$ strip of Cu foil was placed in the higher constant-temperature zone (~1050 °C) and the dielectric substrates were spaced in the lower constant-temperature zone (600 °C). The furnace was heated and pumped to 1.0×10^{-6} Torr. The Cu foil surrounding the quartz tube was annealed at the growth temperature under flowing hydrogen (50 sccm) for 20 min to remove the remaining copper oxide. Subsequently, methane was added in a 2:1 methane-to-hydrogen ratio for 60 min growth. After growth, the furnace was cooled down to room temperature quickly by simply opening the furnace.

Following growth, the morphology of the sample was characterized with the use of a scanning electron microscope (SEM, Zeiss Gemini Ultra-55) and transmission electron microscope (TEM, JEM-2100F). Raman spectra were obtained with a Horiba HR800 Raman microscopy system (laser wavelength 473 nm and laser spot size about 0.5 mm). The transmittance of the sample was measured using a spectrophotometer (DONGGANG, UV-4501) where a bare quartz substrate was used as a reference. The resistance of the sample was measured by depositing the silver electrode on the surface. Other characterization methods include x-ray photoelectron spectroscopy (XPS, ThermoFisher SCIENTIFIC ESCALAB 250).

3. Results and discussion

High-quality monolayer graphene can be grown on the polished SiO_2 substrate. The optical image of the sample (figure 2(a)) shows uniform color and no large wrinkles, which is distinctly different from that grown on Cu foils. To better illustrate the surface features of the sample,

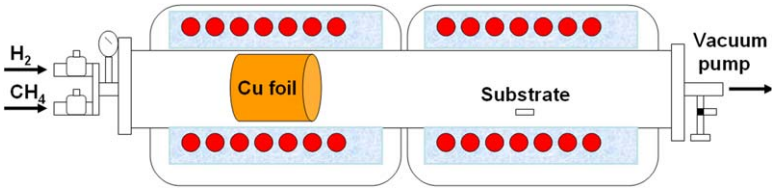

Figure 1. Schematic diagram of the growth of graphene and graphene-CNTs by CVD using a two-heating reactor.

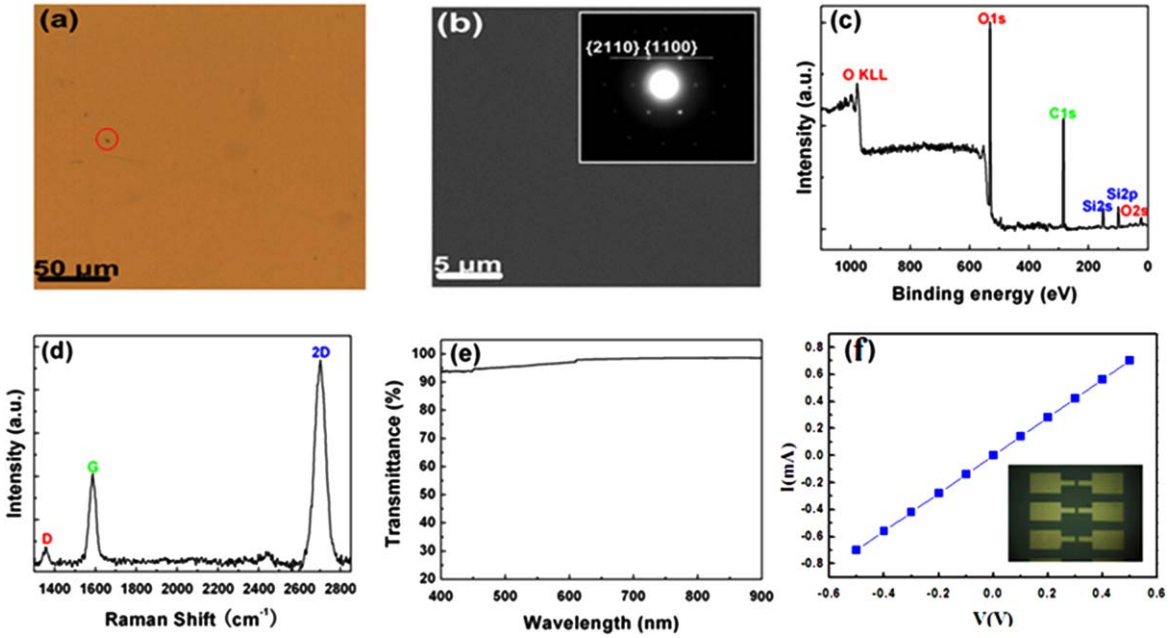

Figure 2. (a)–(f) are, respectively, the optical image, SEM image (Inset: SAED patterns), XPS survey spectrum, Raman spectrum, transmittance spectrum and the *I*–*V* curve of the graphene film directly grown on the polished SiO_2 substrate.

SEM was conducted on the sample. Even under a high magnification, a uniform coverage is still appreciated (figure 2(b)). SAED patterns (inset of figure 2(b)) show the typical sixfold symmetry structure of graphene [28]. As can be seen, the inner peaks {1100} are more intense than the outer ones {2110}, which is regarded as the typical characteristic of monolayer graphene [29]. It should be stressed that after the CVD growth, the Cu element is not detected within the detectable resolution limit (figure 2(c)). This phenomenon can also be demonstrated by the optical image of the quartz tube used in this case (figure 3). As shown in the image, the evaporated Cu atoms are deposited on the region between the lower constant-temperature zone and the higher constant-temperature zone, closer to the later one. The Raman spectrum of the sample randomly collected is shown in figure 2(d). The spectrum reveals the presence of D, G, and 2D bands at ~1350, ~1582 and ~2700 cm^{-1}, respectively, which are the signatures of graphene. Typical features of monolayer graphene: a symmetric 2D band with a FWHM of 34 cm^{-1} and the ratio of the band intensities of the 2D band to the G band ($I_{2D}/I_G \sim 2.2$) are also shown in figure 2(d). The low value of the ratio $I_D/I_G \sim 0.15$ indicates that the prepared

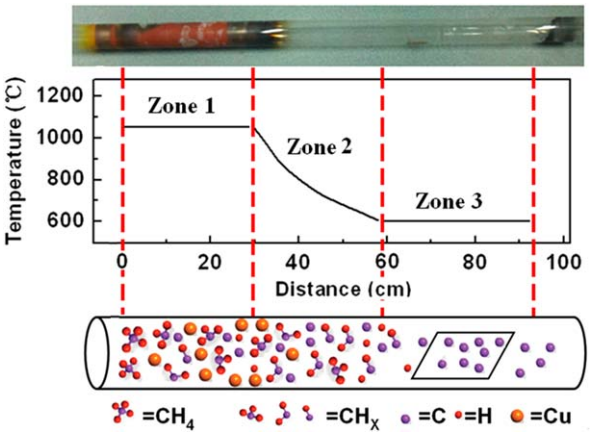

Figure 3. The optical image of the quartz tube used in this CVD route, calibration of the temperature profile along the quartz tube and schematic illustration of graphene growth mechanism.

graphene features a relatively low defect density. These Raman results confirm that high-quality monolayer graphene can be deposited using this method.

Figure 2(e) shows the transmission spectrum of graphene deposited on the polished SiO_2 substrate. As can be seen, the transmission of the graphene film holds the value ~97% at the wavelength of 550 nm, which is similar to that of the monolayer graphene [30]. We also measured the sheet resistance (R_s) of the prepared graphene film (figure 2(f)) obtained at room temperature. The calculated average value of the R_s is $\sim 700\,\Omega\,\square^{-1}$. The excellent optical and electrical properties further demonstrate that high-quality graphene can be prepared using a two-heating reactor CVD system in a relatively low temperature.

We propose a mechanism for direct deposition of graphene on the lower-temperature substrates. To understand the mechanism of graphene growth by using such a revised CVD system, three zones with different temperatures are divided due to the temperature gradient: higher constant-temperature zone (1), gently declined temperature zone (2) and lower constant-temperature zone (3). Two constant-temperature zones (1 and 3) are obtained by the two-heating reactor, in which the temperature can be controlled independently. Figure 3 shows the optical image of the quartz tube used in this CVD route, calibration of the temperature profile along the quartz tube and schematic illustration of the graphene growth mechanism. There are several processes existing in each zone. At zone (1), thermal dissociation of methane, copper evaporation from the copper foil and deposition on the quartz tube exist. A higher temperature (~1050 °C) is required in our experiment. As we know, thermal dissociation of methane is facile at a temperature above 1000 °C, especially where the Cu catalyst is presented. However, it is hard to proceed at a low temperature below 600 °C, even though the Cu catalyst is presented. The copper foil (or other metal catalyst) is useful in our research. As is well known, thermal dissociation of methane is described as [31] $CH_4 = C + 2H_2 (\Delta H = 75.6\ \text{kJ mol}^{-1})$. The reaction lightly occurs at ⩾300 °C and becomes almost thorough at ⩾1300 °C. The dissociation of hydrocarbon is endothermic and enhanced when a metal catalyst is present. Three intermediates, namely, CH_3, CH_2, and CH, in the reaction are formed in the dehydrogenation steps. All four dehydrogenation steps are endothermic, and the corresponding activation energy

barriers are about 1.0–2.0 eV. Therefore, sufficient Cu atoms which cause the complete dehydrogenation of methane play a crucial role [32].

A small quantity of Cu atoms can be evaporated from the Cu foil surface by the higher temperature (1050 °C), which is close to the Cu melting point (1084 °C). Some of the evaporated Cu atoms will float with the gas flow, though most of them are deposited on the quartz tube surface, as shown in figure 3. Fortunately, different from the one-temperature CVD reactor, the temperature of zone (2) between the two constant-temperature zones (1 and 3) declines gently. This gently declined temperature can make the evaporated Cu atoms deposit on the region close to the higher constant-temperature zone (1). The carbon species may also deposit on this region, but most of them will float to the lower constant-temperature zone (3). Carbon black is even seen on the left region of the quartz tube. At the same time, the thermal dissociation of hydrocarbon is still processing, more and more carbon atoms can be formed and float to zone (3). At zone (3), the graphene growth process on the substrate surface is the most complicated one, involves the coalescence of the active species, their nucleation, and finally the formation of graphene. Many researchers have already studied many relevant elementary reactions, such as incorporation of atomic carbon [33] and the combination of CH groups [34]. In fact, carbon black was also observed at zone (3), which was introduced in the growth process. In our experiments, the polished SiO_2 substrates were located on the same region with the same tube and synthesis condition. Consequently, after several times, the carbon black formed on the location of the tube. In summary, the higher constant-temperature zone offers enough power for the dissociation of methane and the lower constant-temperature zone makes the decomposed carbon atoms deposit readily on the substrate. Meanwhile, the distinct form of the temperature variation effectively controls the regions where the evaporated Cu atoms and the decomposed carbon atoms deposit.

In our case, the graphene films are predominantly monolayer and the growth process is self-limited. This is probably as SiO_2 has a higher surface energy than after it is covered by graphene. Namely, the cohesion energy between SiO_2 and graphene is higher than that of graphene-to-graphene [35]. Therefore, after being covered by a layer of graphene, the carbon species become hard to nucleate on the graphene covered area due to the relatively weak cohesion energy, refusing to form the second layer [36]. But, one exception occurs at the defects where the dangling bonds give more opportunities for carbon adsorption to form the bilayer or multilayer graphene. Very few domain-like structures (darker color, in the red circle) can be detected in figure 2(a), in spite of them occupying only a small fraction of the whole region.

If the 'defects' are big enough, most of the carbon atoms will be grown on these active catalytic sites. Wire-type nanostructures (such as carbon nanotubes) may be formed on such active catalytic sites. In our study, SiO_2 nanodots can be used as the active catalytic site for the synthesis of the CNTs. The graphene-CNTs hybrid is fabricated on the unpolished SiO_2 substrate with many SiO_2 nanodots. The other growth conditions (the location of the substrate, the growth temperature and the flow of the gases) are the same as that presented above.

As shown in figure 4(a), a large-area and the dense CNTs (average length is ~2 μm) on top of the graphene film are obtained on the unpolished SiO_2 substrate. It is also possible to investigate the state of the graphene-CNT hybrids transferred to a small holey copper grid using TEM. Figure 4(b) shows an image of coexisted graphene and CNTs, which is well consistent with the SEM result. As seen in the high-resolution TEM image of the hybrid (figure 4(c)), the average diameter of the CNTs is ~5.8 nm and the measured graphitic interlayer spacing is

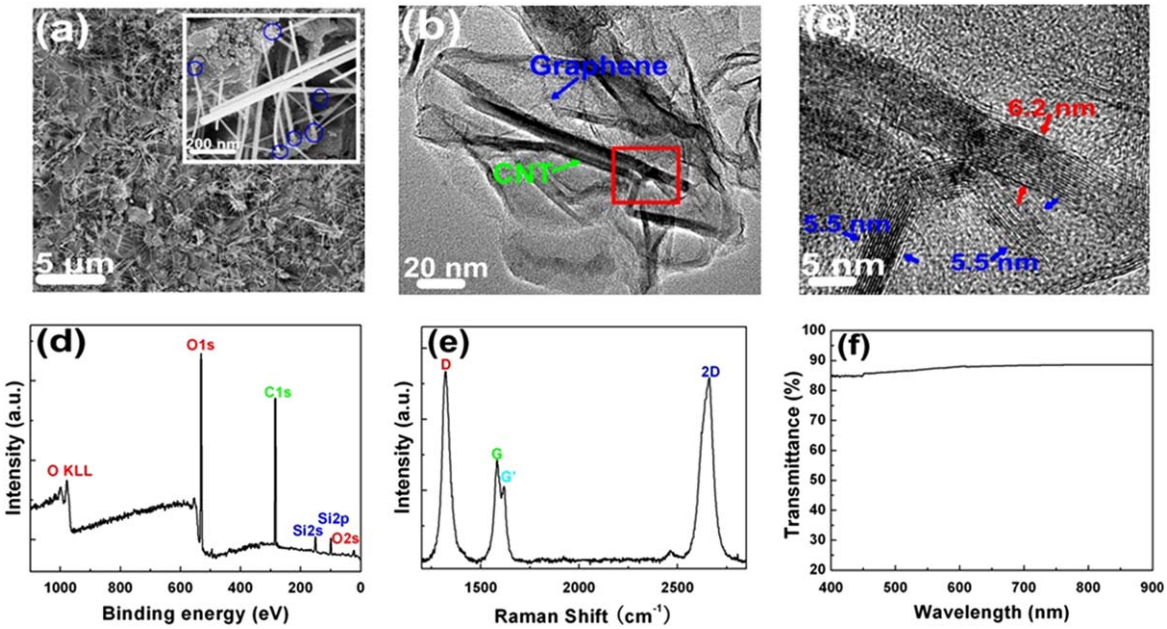

Figure 4. (a)–(e) are, respectively, the SEM image (Inset: magnified SEM image), TEM image, high-resolution TEM image (taken from the position marked with the red box in 4b), XPS survey spectrum, Raman spectrum and transmittance spectrum of graphene-CNTs hybrid directly grown on the unpolished SiO_2 substrate by two-heating reactor CVDs.

~0.34 nm, which is consistent with the previous report on the CNTs [37–39]. We also conducted Raman observations on the as-grown sample. A typical Raman spectrum of a graphene-CNTs hybrid is shown in figure 4(e), which displayed all the typical bands (G, G', D and 2D) of a carbon nanostructure. Besides two characteristic peaks (~1582 and 2665 cm^{-1}) of sp^2 carbon materials, a weak peak (~1618 cm^{-1}) beside the G band is present, which can be assigned to the G' band of the CNTs [21], which provides good evidence for the coexistence of CNTs and graphene. Figure 4(f) shows the optical transmission spectrum as a function of wavelength for the graphene-CNTs hybrid film. The transmission of the graphene-CNTs holds the value ~87% at the wavelength of 550 nm, which is smaller than that (97%) of the graphene (figure 2(e)). This reduction of the transmission can be attributed to the fact that the CNTs are grown on the graphene surface, which can be demonstrated from figure 4(b). The measurements of sheet resistance on the graphene-CNT hybrids were also conducted in different areas. The average value of R_s is ~510 $\Omega\,\square^{-1}$, which is lower than that (~700 $\Omega\,\square^{-1}$) of the graphene. To explain the improvement in R_s of the graphene-CNT hybrids, we suggest that CNTs acting as wires can perfectly connect the large graphene pads together.

It should be stressed that after the CVD growth, no Cu element is detected within the detectable resolution limit (figure 4(d)), which demonstrates that the Cu nanoparticles may not be the active catalytic sites for the formation of the graphene-CNT hybrids. This phenomenon can be proved by the fact that Cu nanoparticles have been deposited on zones (1) and (2). We believed that the SiO_2 nanodots on the unpolished SiO_2 substrate play an important role in the graphene-CNTs hybrid formation during such CVD process. The inset of figure 4(a) provides

an SEM image of the CNTs, which illustrates the CNTs are stemmed from SiO_2 nanodots, which can act as active catalytic sites for the growth of CNTs [40, 41].

In order to further investigate the effects of the substrates on the synthesis of the graphene and graphene-CNT hybrids in this case, we set up a series of synthesis experiments on various substrates. $SiO_{2(HF)}$, $Si_{(NaOH)}$ and glass fibers are used as the substrate. The other growth conditions are the same as that presented above. The unpolished SiO_2 was treated with HF (wt 5%) for 5 min in the room temperature, conveniently we referred it as $SiO_{2(HF)}$. The 200 μm thick monocrystalline Si was treated in a mixed solution (NaOH wt 3% and isopropyl alcohol wt 5%) in 78 °C, for convenience we referred to it as $Si_{(NaOH)}$.

SEM was used to investigate the morphology of the samples before and after the CVD growth. The surface of the $SiO_{2(HF)}$ substrate before the CVD growth (figure 5(a)) exhibits a relatively smooth structure with some crystal defects. After the CVD growth, the $SiO_{2(HF)}$ substrate still presents a relatively smooth structure covered by graphene except in the regions with crystal defect (figure 5(d)). The eyelash-like CNTs arranged in parallel are detected in the region with crystal defect. This phenomenon indicates that the crystal defects can act as the active catalytic sites for the growth of CNTs. Raman spectra were conducted on the samples, which is taken randomly from the deposited sample. As shown in figure 5(g), the Raman profile includes the feature peaks of graphene. Two characteristic peaks at ~1582 and ~2700 cm^{-1}, respectively, assigned to the G and 2D band of sp^2 carbon materials are detected and the characteristic peak (~1618 cm^{-1}) of the CNTs is not observed. These Raman results are well consistent with the observation from the SEM image and further suggest that the large-area CNTs cannot be fabricated on the relatively smooth substrate by this two-heating reactor. Even though the eyelash-like CNTs are detected by the SEM in the region with crystal defect on the $SiO_{2(HF)}$ substrate, the amount of these eyelash-like CNTs is too small to be observed by the Raman spectra. Typical SEM image of the $Si_{(NaOH)}$ substrate before the CVD growth is shown in figure 5(b). It can be seen from the image that there is a pyramid-like structure on the surface of the $Si_{(NaOH)}$ substrate. It can be ascribed to the anisotropic etching property of silicon in the NaOH solution. The $Si_{(NaOH)}$ substrate is covered by the carbon amorphous layers with carbon nanodots after the treatment in the CVD furnace (figure 5(e)). Figure 5(h) exhibits the Raman spectrum of the $Si_{(NaOH)}$ substrate after the CVD growth. A disordered D band, located around 1350 cm^{-1}, and an active graphite G band, located around 1600 cm^{-1}, were observed. However, a 2D band (~2700 cm^{-1}) related to a graphene layer structure is hardly observed, which indicates that the $Si_{(NaOH)}$ substrates are covered by many carbon amorphous layers instead of the graphene or CNTs after the CVD treatment. These results suggest that the substrates play a crucial role in the fabrication process of the graphene and graphene-CNT hybrids. The smooth substrate is adaptive for the direct CVD gowth of graphene by this two-heating reactor. The SiO_2 nanodots and crystal defects can act as the catalyst sites for the growth of CNTs. The substrates with high surface flatness are not adaptive for the formation of graphene-CNT hybrids. What is more, the SiO_2 base is better qualified to serve as the substrate for graphene and graphene-CNT hybrids growth than the Si base, which can be attributed to the fact that the presence of oxygen can enhance the adsorption of carbon atoms on the SiO_2 base.

Figures 5(c) and (f) show the typical SEM images of the glass fiber before and after the CVD growth. The carbon atoms cover the glass fiber to form the graphene and graphene-CNT hybrids. The carbon atoms are easily deposited and grown on the overlap region of the glass fiber, shown in the inset of figure 5(f). The overlap region and the top of the glass fiber can act as the catalyst sites for the further growth of the graphene and graphene-CNT hybrids. As we all

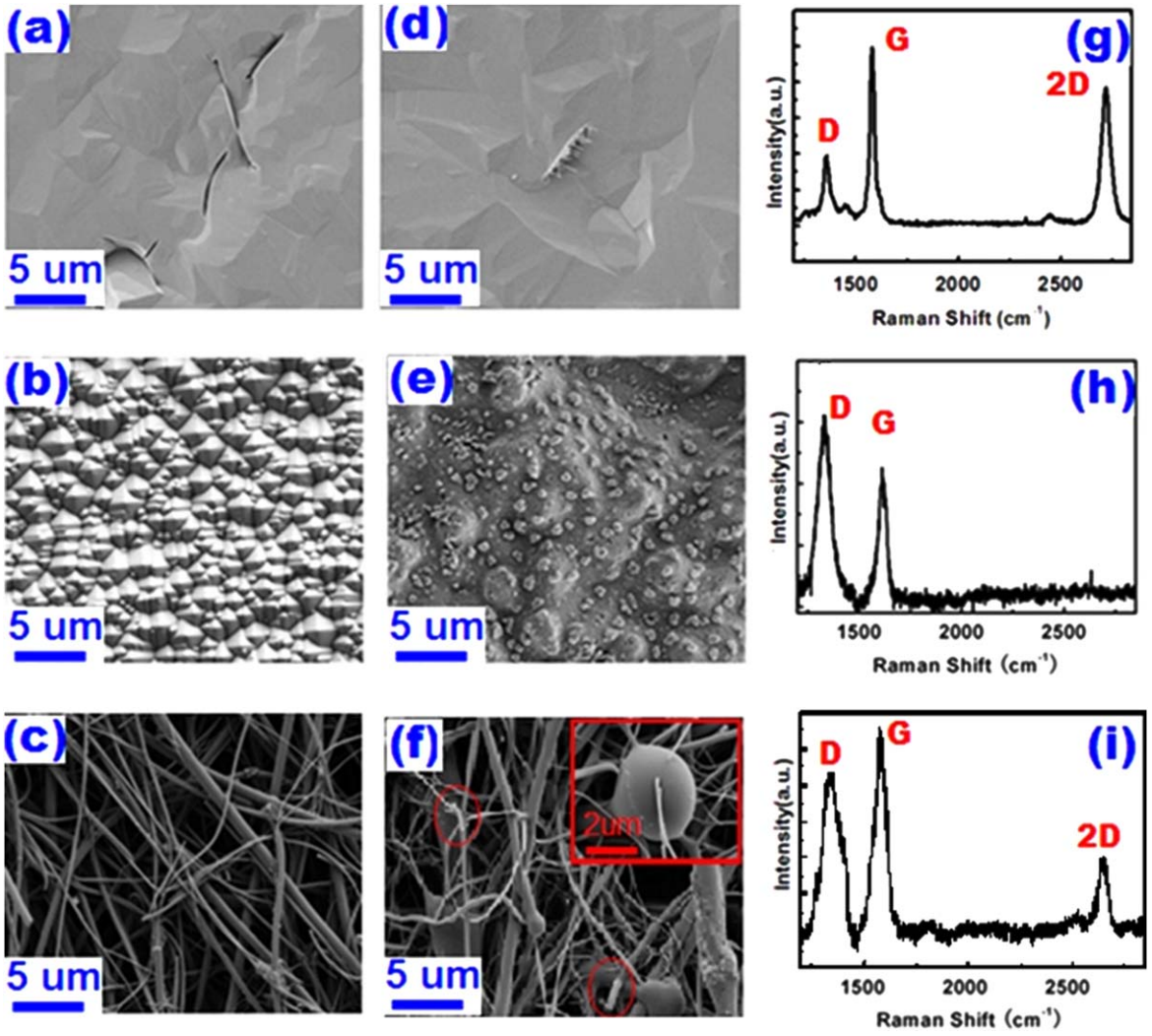

Figure 5. (a), (b) and (c) are, respectively, the SEM images of the $SiO_{2(HF)}$, $Si_{(NaOH)}$ and glass fiber substrates before the CVD growth. (d), (e) and (f) are, respectively, the SEM images of the $SiO_{2(HF)}$, $Si_{(NaOH)}$ and glass fiber substrates after the CVD growth. (g), (h) and (i) are, respectively, the Raman spectra of the $SiO_{2(HF)}$, $Si_{(NaOH)}$ and glass fiber substrates after the CVD growth.

know, the brightness of the SEM images depends on the conductivity of the substrate materials. As shown in the red circle of figure 5(f), the top of the glass fiber is much brighter than other areas. Carbon nanotubes may be synthesized on some of the glass fiber top and overlap region. Figure 5(i) exhibits the Raman spectrum of the glass fiber substrate after the CVD growth. A disordered D band, located around 1350 cm^{-1}, and an active graphite G band, located around 1600 cm^{-1}, were observed. 2D band (~2700 cm^{-1}) related to a graphene layer structure is also observed, which indicates the carbon based nanomaterials are sp^2 structure materials. We believed that several layered graphene is grown on the surface and the CNTs are formed on the top and overlap region of the glass fiber. The sheet resistances of the fabricated samples have been measured as 550, 120 and 180 $\Omega\,\square^{-1}$ for the $SiO_{2(HF)}$, $Si_{(NaOH)}$ and glass fiber substrate.

The lower sheet resistance of the $Si_{(NaOH)}$ and glass fiber samples are caused by more layers of the carbon atoms.

4. Conclusions

We have demonstrated the facile growth of graphene and graphene-CNT hybrids using a two-heating reactor. The morphology and electrical properties of the nanostructures have been analyzed with the effects of the substrate surface. A relatively flat surface is beneficial for the synthesis of graphene. Bigger 'defects', such as nanodots, can be used as the catalyst sites for the further growth of the CNTs. These results demonstrate that the method presented here provides a promising and high-efficiency technique to directly synthesize various carbon nanostructures.

Acknowledgements

The authors are grateful for the financial support from the National Natural Science Foundation of China (11274204, 61205174 and 61307120), Specialized Research Fund for the Doctoral Program of Higher Education of China (20133704120008), Shandong Excellent Young Scientist Research Award Fund (BS2012CL034), Shandong Province Higher Educational Science and Technology Program (J12LA07) and Science and Technology Planning Project of Higher Education of Shandong Province (J11LA14).

Reference

[1] Chang H and Wu H 2013 Graphene-based nanomaterials: synthesis, properties, and optical and optoelectronic applications *Adv. Funct. Mater.* **23** 1984–97
[2] Orbaek A W, Owens A C, Crouse C C, Pint C L, Hauge R H and Barron A R 2013 Single walled carbon nanotube growth and chirality dependence on catalyst composition *Nanoscale* **5** 9848–59
[3] Terrones M *et al* 1997 Controlled production of aligned-nanotube bundles *Nature* **388** 52–5
[4] Wan D Y, Lin T Q, Bi H, Huang F Q, Xie X M, Chen I W and Jiang M H 2012 Autonomously controlled homogenous growth of wafer-sized high-quality graphene via a smart janus substrate *Adv. Funct. Mater* **22** 1033–9
[5] Journet C, Mase W K, Bernier P, Loiseau A, Chapelle M L, Lefrant S, Deniard P, Lee R and Fischer J E 1997 Large-scale production of single-walled carbon nanotubes by the electric-arc technique *Nature* **388** 756
[6] Neyts E C, Duin A and Bogaerts A 2011 Changing chirality during single-walled carbon nanotube growth: A reactive molecular dynamics/monte carlo study *J. Am. Chem. Soc.* **133** 17225–31
[7] Isborn C M, Tang C, Martini A, Johnson E R, Otero-de-la-Roza A and Tung V C 2013 Carbon nanotube chirality determines efficiency of electron transfer to fullerene in all-carbon photovoltaics *J. Phys. Chem. Lett.* **4** 2914–8
[8] Cao J, Nyffeler C, Lister K and Lonescu A M 2012 Resist-assisted assembly of single-walled carbon nanotube devices with nanoscale precision *Carbon* **50** 1720–6
[9] Wang Q H, Setlur A A, Lauerhaas J M, Dai J Y, Seelig E W and Chang R P 1998 A nanotube-based field-emission flat panel display *Appl. Phys. Lett.* **72** 2912–3
[10] Han S, Maune H T, Barish R D, Bockrath M and Goddard W A 2012 DNA-linker-induced surface assembly of ultra dense parallel single walled carbon nanotube arrays *Nano Lett.* **2** 1129–35

[11] Frank S, Poncharal P, Wang Z L and Heer W A 1998 Carbon nanotube quantum resistors *Science* **280** 1744–6
[12] Ebbesen T W 1997 *Carbon Nanotubes: Preparation and Properties* (Boca Raton, FL: CRC Press)
[13] Mukhopadhyay A, Guo F, Tokranov A, Xiao X C, Hurt R H and Sheldon B W 2013 Engineering graphene layer orientation to attain high rate capability and anisotropic properties in Li-ion cattery electrodes *Adv. Funct. Mater.* **23** 2397–404
[14] Schedin F, Geim A K, Morozov S V, Hill E W, Blake P, Katsnelson M I and Novoselov K S 2007 Detection of individual gas molecules adsorbed on graphene *Nat. Mater.* **6** 652–5
[15] Li X L, Zhang G Y, Bai X D, Sun X M, Wang X R, Wang E and Dai H J 2008 Chemically derived, ultrasmooth graphene nanoribbon semiconductors *Science* **319** 1229–32
[16] Seo J W, Jun Y W, Park S W, Nah H, Moon T, Park B, Kim J G, Kim Y J and Cheon J 2007 Two-dimensional nanosheet crystals *Angew. Chem. Int. Ed.* **46** 8828–31
[17] Stoller M D, Park S J, Zhu Y W, An J H and Ruoff R S 2008 Graphene-based ultracapacitors *Nano Lett.* **8** 3498–502
[18] Li C Y, Li Z, Zhu H W, Wang K L, Wei J Q, Li X, Sun P Z, Zhang H and Wu D H 2010 Graphene nano-'patch' on a carbon nanotube network for highly transparent/conductive thin film applications *J. Phys. Chem.* C **114** 14008–12
[19] Das S, Seelaboyina R, Verma V, Lahiri I, Hwang J Y, Banerjee B and Choi W 2011 Synthesis and characterization of self-organized multilayered graphene–carbon nanotube hybrid films *J. Mater. Chem.* **21** 7289–95
[20] Seo S D, Hwang I S, Lee S H, Shim H W and Kim D W 2012 1D/2D carbon nanotube/graphene nanosheet composite anodes fabricated using electrophoretic assembly *Ceram. Int.* **38** 3017–21
[21] Dong X C, Li B, Wei A, Cao X H, Chan-Park M B, Zhang H, Li L J, Huang W and Chen P 2011 One-step growth of graphene–carbon nanotube hybrid materials by chemical vapor deposition *Carbon* **49** 2944–9
[22] Jiang H, Lee P S and Li C 2013 3D carbon based nanostructures for advanced supercapacitors *Energy Environ. Sci.* **6** 41–53
[23] Xie X Y, Zhang C, Wu M B, Tao Y, Lv W and Yang Q H 2013 Porous MnO2 for use in a high performance supercapacitor: replication of a 3D graphene network as a reactive template *Chem. Commun.* **49** 11092–4
[24] Seo J, Lee T J, Ko S, Yeo H, Kim S, Noh T, Song S, Sung M M and Lee H 2012 Hierarchical and multifunctional three-dimensional network of carbon nanotubes for microfluidic applications *Adv. Mater.* **24** 1975–9
[25] Duarte R M, Alanis F C, Renaud P and Ros A 2013 Dielectrophoresis of lambda-DNA using 3D carbon electrodes *Electrophoresis* **34** 1113–22
[26] Qin G H, Xue S, Ma Q Q and Wang C Y 2014 The morphology controlled synthesis of 3D networking LiFePO4 with multiwalled-carbon nanotubes for Li-ion batteries *CrystEngComm* **16** 260–9
[27] Cao X H, Shi Y M, Shi W H, Rui X H, Yan Q Y, Kong J and Zhang H 2013 Preparation of MoS2-coated three-dimensional graphene networks for high-performance anode material in Lithium-ion batteries *Small* **9** 3433–8
[28] Meyer J C, Geim A K, Katsnelson M I, Novoselov K S, Booth T J and Roth S 2007 The structure of suspended graphene sheets *Nature* **446** 60–3
[29] Hernandez Y *et al* 2008 High-yield production of graphene by liquid-phase exfoliation of graphite *Nat. Nanotechnol.* **3** 563–8
[30] Zhang C, Man B Y, Yang C, Jiang S Z, Liu M, Chen C S, Xu S C, Sun Z C, Gao X G and Chen X J 2013 Facile synthesis of graphene on dielectric surfaces using a two-temperature reactor CVD system *Nanotechnology* **24** 395603
[31] Kozlov G I and Knorre V G 1962 Single-pulse shock tube studies on the kinetics of the thermal decomposition of methane *Combust. Flame* **6** 253–63

[32] Kim H, Song I, Park C, Son M, Hong M, Kim Y, Kim J S, Shin H J, Baik J and Choi H C 2013 Copper-vapor-assisted chemical vapor deposition for high-quality and metal-free single-layer graphene on amorphous SiO_2 substrate *ACS Nano* **7** 6575–82

[33] Wu P, Zhang W, Li Z, Yang J and Hou J G 2010 Coalescence of carbon atoms on Cu (111) surface Emergence of a stable bridging-metal structure motif *J. Chem. Phys.* **133** 071101

[34] Zhang W, Wu P, Li Z and Yang J 2011 First-principles thermodynamics of graphene growth on Cu surfaces *J. Phys. Chem.* C **115** 17782–7

[35] Koenig S P, Boddeti N G, Dunn M L and Bunch J S 2011 Ultrastrong adhesion of graphene membranes *Nat. Nanotechnol.* **6** 543–6

[36] Xu S C, Man B Y, Jiang S Z, Chen C S, Yang C, Liu M, Gao X G, Sun Z C and Zhang C 2013 Direct synthesis of graphene on SiO2substrates by chemical vapor deposition *CrystEngComm* **15** 1840–4

[37] Woo Y S, Jeon D Y, Han I T, Park Y J, Kim H J, Jung J E, Kim J M and Lee N S 2003 Structural characteristics of carbon nanorods and nanotubes grown using electron cyclotron resonance chemical vapor deposition *J. Appl. Phys.* **94** 6789

[38] Irie M, Nakamura M, Zhang M, Yuge R, Iijima S and Yudasaka M 2010 Quantification of thin graphene sheets contained in spherical aggregates of single-walled carbon nanohorns *Chem. Phys. Lett.* **500** 96–9

[39] Zhang M and Li J 2009 Carbon nanotube in different shapes *Mater. today* **12** 12–18

[40] Liu B L, Ren W C, Gao L B, Li S S, Pei S F, Liu C, Jiang C B and Cheng H M Metal-catalyst-free growth of single-walled carbon nanotubes *J. Am. Chem. Soc.* **131** 2082–3

[41] Huang S M, Cai Q R, Chen J Y, Qian Y and Zhang L J 2009 Metal-catalyst-free growth of single-walled carbon nanotubes on substrates *J. Am. Chem. Soc.* **131** 2094–5